UDK 669.1.017:620.172
Original scientific article/Izvirni znanstveni članek

ISSN 1580-2949
MTAEC9, 57(4)367(2023)

HOT-DEFORMATION BEHAVIOR AND PROCESSING MAP OF 22MnB5 HIGH-STRENGTH STEEL

VROČA DEFORMACIJA IN PROCESNA MAPA JEKLA Z VISOKO TRDNOSTJO TIPA 22MnB5

Hongchao Ji[1*], Yanke Wen[1], Guofa Cui [2], Weichi Pei[1], Wenchao Xiao[3]

[1]College of Mechanical Engineering, North China University of Science and Technology, Tangshan, 063210 China.
[2]Tangshan Longquan Machinery Co., Ltd., Tangshan, Hebei, 063210.
[3]Shenzhen Institute for Advanced Study, University of Electronic Science and Technology of China, Shenzhen, 518000, Guangdong, China.

Prejem rokopisa – received: 2023-05-05; sprejem za objavo – accepted for publication: 2023-06-26

doi:10.17222/mit.2023.874

In order to explore the hot formability of 22MnB5, a hot-tensile test of 22MnB5 high-strength steel plate was carried out using a Gleeble-1500 hot-tensile-testing machine. The stress-strain curves at 850 °C to 950 °C and 0.01 s^{-1} to 10 s^{-1} were obtained. The results show that 22MnB5 has an obvious positive-strain-rate sensitivity, and its peak stress decreases with the increase of temperature. The mechanical constitutive equation of 22MnB5 was established by using the improved Johnson-Cook model, and the fitting value was compared with the experimental value. Based on the dynamic material model, the hot-processing map of 22MnB5 was established and analyzed. The hot-processing process was determined as follows: deformation temperature 880 °C to 930 °C, strain rate 0.01 s^{-1} to 1 s^{-1}.

Keywords: 22MnB5 high-strength steel, hot-deformation behaviour, J-C constitutive model, processing map

V članku je opisana raziskava vroče preoblikovalnosti jekla vrste 22MnB5 s pomočjo vročih nateznih preizkusov izvedenih na preizkusni napravi Gleeble-1500. Preizkušance izrezane iz jeklenih plošč so segreli na temperature med 850 °C in 950 °C, jih deformirali s hitrostjo deformacije 0,01 s^{-1} do 10 s^{-1} in izdelali odgovarjajoče krivulje napetost-deformacija. Rezultati preiskav so pokazali, da je visoko trdno jeklo 22MnB5 ustrezno občutljivo na hitrost deformacije in da se maksimalna napetost deformacije zmanjšuje z naraščajočo temperaturo preizkusov. Avtorji so s pomočjo izboljšanega Johnson-Cookovega modela določili mehansko konstitutivno enačbo deformacijskega obnašanja izbranega jekla pri povišanih temperaturah in dobljene vrednosti primerjali z eksperimentalnimi. Nato so na osnovi dinamičnega materialnega modela izdelali in analizirali procesno mapo izbranega jekla vrste 22MnB5. Ugotovljeni optimalni proces vroče deformacije poteka v temperaturnem območju med 880 °C in 930 °C pri hitrostih deformacije med 0,01 s^{-1} in 1 s^{-1}.

Ključne besede: visoko trdno jeklo vrste 22MnB5, obnašanje jekla med vročo deformacijo, izboljšan J-C konstitutivni model, procesna mapa

1 INTRODUCTION

In recent years, high-strength steel has become the preferred material for lightweight bodies because of its high strength, corrosion resistance, ductility and stability. High-strength steel is more often used to manufacture the structural components of the car body, such as A-pillar, B-pillar, anti-collision beam and underframe.[1–3] As a high-strength steel, 22MnB5 is widely used in body parts because of its excellent performance. The use of high-strength materials can effectively reduce the body's weight under the premise of meeting the safety requirements. Light weight has become the trend in the development of the automotive industry.[4,5]

The thermal deformation process is accompanied by microstructure evolution. It is necessary to study the formation mechanism of hot processing and establish a constitutive model to characterize the correlation between flow stress and microstructure.[6,7] The thermal deformation of metal in the hot-forming process is often complex, and the influence of process parameters on the thermal deformation and mechanical properties of metal is significant.[8,9] Lin et al.[10] obtained the stress-strain relationship of a Al-Si-Mg alloy according to the hot-compression test and established a constitutive model to predict its flow stress. The microstructure observation proved that the main reason for its flow instability was the local, uneven deformation of the eutectic silicon phase at a low forming temperature and a high strain rate, the formation of an adiabatic shear band and brittle fracture. The best hot-processing parameters are obtained by using the hot-processing map. Turetta A et al.[11] analysed the influence of process parameters on the formability of 22MnB5 sheet during hot stamping, studied the relationship between the change of austenite microstructure size and time, and found the best austenitizing temperature of the sheet is 900 °C. In order to study the flow stress of 22MnB5 steel under high-temperature conditions, Zhou et al.[12] derived and compared the advantages and disadvantages of Arrhenius and unified viscoplastic constitutive models. By comparison, it is found that the Arrhenius constitutive equation has higher accuracy in terms of relative error. It has high ref-

*Corresponding author's e-mail:
jihongchao@ncst.edu.cn

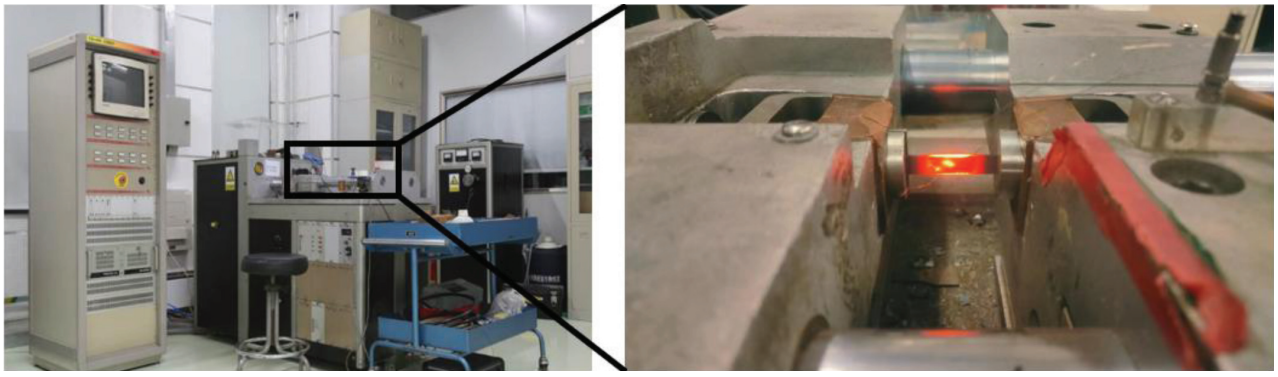

Figure 1: Gleeble-1500 thermal simulation testing machine

erence significance for 22MnB5 high-strength steel in constitutive fitting.

There are few reports on the relationship between hot-deformation behaviour, the hot-deformation constitutive relationship and the hot-processing map of 22MnB5 high-strength steel. In this paper, the tensile test of 22MnB5 high-strength steel at high temperature was carried out using a Gleeble-1500 thermal simulation test machine. Considering the factors of temperature, strain rate and strain, the improved Johnson-Cook constitutive model was used to describe the flow-stress equation, and the experimental data were mild and good. The hot-processing map was constructed to obtain a suitable hot-processing process range, which provided the basis for the hot-stamping-process selection of 22MnB5 high-strength steel.

2 EXPERIMENTAL PART

2.1 Hot-tensile test

The test material is 22MnB5 plate, and its chemical composition is shown in Table 1. The hot-tensile test was carried out using a Gleeble-1500 thermal simulation testing machine, and the equipment is shown in **Figure 1**.

Table 1: Chemical composition of 22MnB5

Component	C	Mn	Si	Al	Ti	Cr	B	Fe
w/%	0.22	1.20	0.20	0.02	0.03	0.20	0.0035	Bal.

The specimen size is shown in **Figure 2a**. The thickness is 2 mm. The hot-tensile deformation temperatures are 850 °C, 900 °C and 950 °C, and the strain rates are 0.01 s^{-1}, 0.1 s^{-1}, 1 s^{-1} and 10 s^{-1}. Firstly, the sample was heated to 700 °C at a rate of 15 °C/s, and then heated to 950 °C at a rate of 5 °C/s. After holding for 3 min, the microstructure was completely transformed from ferrite and pearlite to austenite. Then, it was rapidly reduced to the deformation temperature at a rate of 50 °C/s, and held for 10s to improve the uniformity of the temperature. Finally, it was stretched to fracture at different strain rates. **Figure 2b** is a comparison diagram of the test piece before and after stretching.

2.2 Analysis of high-temperature deformation behavior of 22MnB5 plate

Due to the resistance heating of the thermal simulation test machine, the temperature distribution in the length direction is not uniform, and there is a mechanical transmission error, which may cause virtual displacement during the stretching process. In order to reduce the error, a 20-mm middle area is selected as the original gauge in the middle area of the sample to calculate the tensile speed corresponding to the strain rate during the tensile test. The following formula is used to calculate the true stress vs. true strain curve:

$$\varepsilon = \ln\left(\frac{l}{l_0}\right) = \ln\left(1+\frac{\Delta l}{l_0}\right) \quad (1)$$

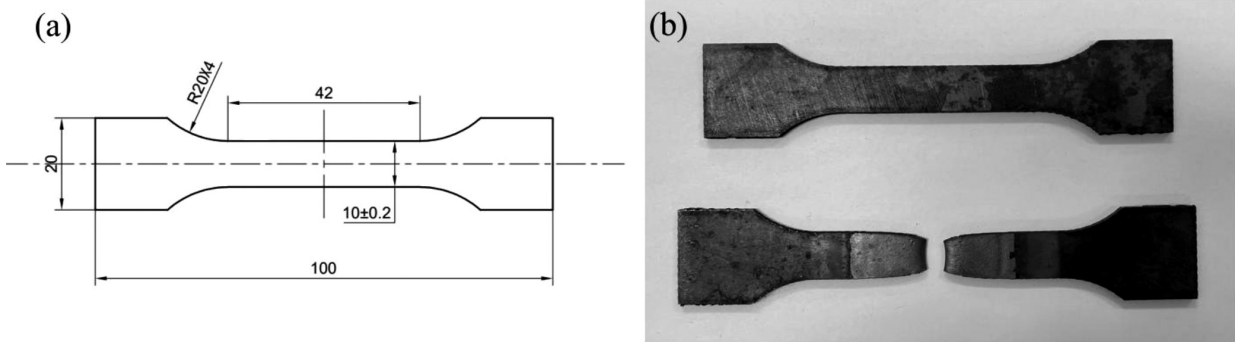

Figure 2: Comparison of sample size before and after stretching: a) sample size, b) stretching comparison diagram

$$\sigma = \frac{F}{A} = \frac{Fl}{A_0 l_0} = \frac{F}{A_0}\left(1 + \frac{\Delta l}{l_0}\right) \quad (2)$$

where, ε and σ are true strain and true stress, A_0 and l_0 are the initial cross-sectional area and initial length of the gauge section, A and l are the transient cross-sectional area and length of the gauge section, Δl is the transient extension length of the gauge section, and F is the transient load size.

The true stress vs. tru strain curves of 22MnB5 high-strength steel plate under different temperatures of 850 °C, 900 °C and 950 °C and strain rates of 0.01 s^{-1}, 0.1 s^{-1}, 1 s^{-1} and 10 s^{-1} were drawn using Origin software, as shown in **Figure 3**. Boron steel has the process of work hardening and dynamic softening during hot deformation. At the beginning of the deformation, the flow stress increases with the increase of strain, and the dislocations continue to proliferate. The interaction between dislocations increases the resistance of the dislocation movement. At the same time, the smaller strain makes the storage energy in the crystal less, and the dynamic recovery process is difficult to carry out. At this time, work hardening dominates. As the strain increases, the storage energy in the crystal gradually increases, and the dynamic softening and strain hardening gradually tend to be balanced. The hardening and softening processes are almost completed at the same time. When the softening and hardening reach dynamic equilibrium, the true stressvs. true strain curve is almost a horizontal line.

2.3 Microstructure observation

The original microstructure and fracture area of the tensile sample were cut, and the microstructure was observed using a LEICA DMi8 inverted optical microscope after grinding, polishing and etching. SEM has the advantages of large magnification and three-dimensional morphology. Therefore, SEM is used to observe the fracture of the high-temperature specimens. The fracture specimens with a deformation temperature of 900 °C and strain of 1 s^{-1} were observed and analysed.

3 RESULTS AND DISCUSSION

3.1 Establishment of 22MnB5 constitutive equation

The improved Johnson-Cook constitutive model of 22MnB5 high-strength steel is based on the experimental data obtained from the above hot-tensile test to estimate the value of Equation (3). The traditional Johnson-Cook constitutive model has a large fitting error for the flow stress at high temperature, so the temperature-sensitivity coefficient D is introduced on the basis of the traditional constitutive model. Firstly, the values of A, B and n are estimated, and then the obtained parameters are substituted into the original equation to obtain the values of C, D and m. The specific form of the Johnson-Cook constitutive model is:

$$\sigma = (A + B\varepsilon^n)(1 + C\ln\dot{\varepsilon}^*)(1 - DT^{*m}) \quad (3)$$

where A, B, n, C and m are the parameters related to the material. A is the initial yield strength of the material at room temperature; B is the work hardening coefficient; n is hardening index; C is the strain rate sensitivity coefficient; D is the temperature sensitivity coefficient; m is the temperature softening index; and σ and ε are the equivalent stress and equivalent plastic strain, respectively. For the equivalent plastic strain rate parameter, #ε takes 0.01 s^{-1}, and the dimensionless temperature parameter is:

$$T^* = \frac{T - T_0}{T_m - T_0} \quad (4)$$

where T_0 is the reference temperature, generally selected as room temperature (25 °C) and T_m is the melting temperature of the material, 1470 °C.

3.1.1 Determination of A, B, n

The initial yield strength, work-hardening coefficient and work-hardening exponent were determined by tensile tests at room temperature. The strain rate during tension is taken as the reference strain rate of 0.01 s^{-1}. At this time $\dot{\varepsilon} = \dot{\varepsilon}_0$, $T = T_0$, so Equation (3) can be simplified as:

$$\sigma = (A + B\varepsilon^n) \quad (5)$$

The true stress vs. true strain curve of 22MnB5 at room temperature is shown in **Figure 4**.

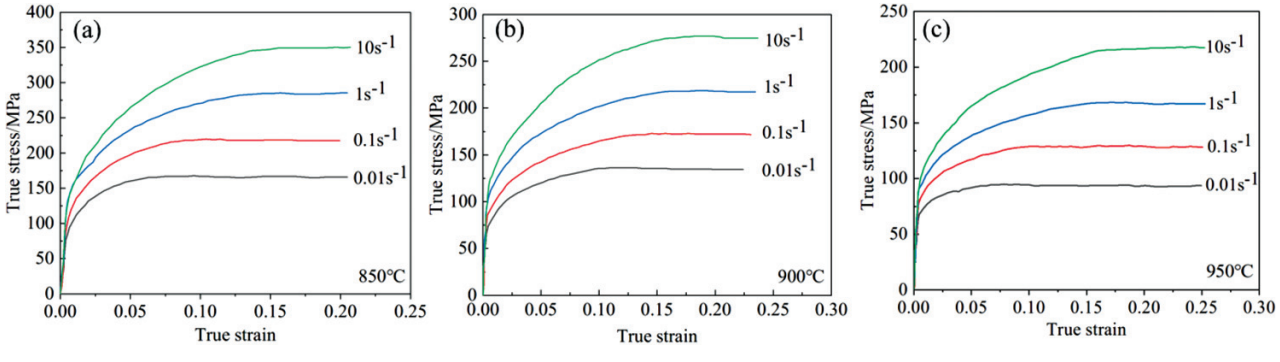

Figure 3: The true stress vs. true strain curves of 22MnB5 at different temperatures and different strain rates

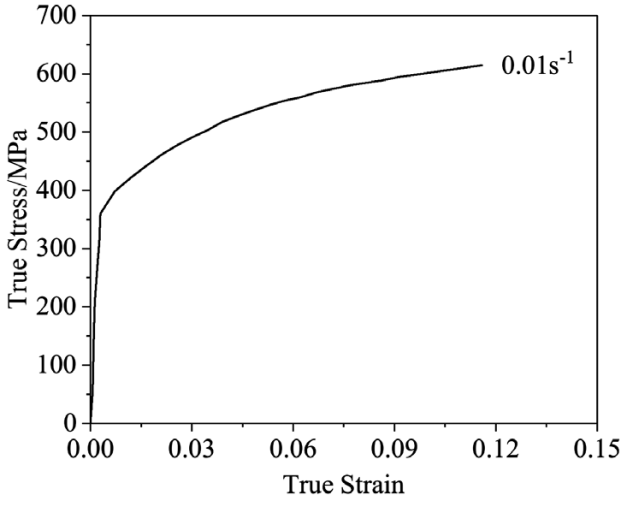

Figure 4: The true stress vs. true strain curve of 22MnB5 at room temperature

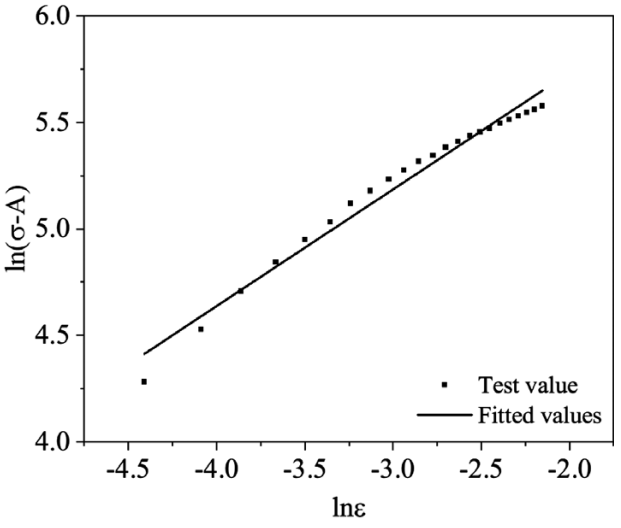

Figure 5: $\ln(\sigma - A) - \ln \varepsilon$ relationship curve

It can be seen from the figure that the stress when the material yields at room temperature is 365 MPa, i.e., the parameter A is 365 MPa. Taking the natural logarithm at both ends of the Equation (5), there are:

$$\ln(\sigma - A) = n \ln \varepsilon + \ln B \tag{6}$$

The values of n and B are obtained by a linear fitting of the stress-strain data in the plastic deformation zone, where n is the slope and intercept. The fitting results are shown in **Figure 5**, n = 0.55, ε = 6.818, B = 914.15. Therefore, the relationship between the flow stress and strain of the material at room temperature is:

$$\sigma = 365 + 914.15\varepsilon^{0.55} \tag{7}$$

The comparison between the experimental and calculated values is shown in **Figure 6**.

3.1.2 Determination of strain-rate sensitivity coefficient C

At the same temperature, the stress-strain curves at different strain rates are studied. At this time, $1 - DT^{*m}$ it is a constant K. Therefore:

$$\frac{\sigma}{K(A + B\varepsilon^n)} = 1 + C \ln \dot{\varepsilon}^* \tag{8}$$

The strain rate is 0.01 s^{-1}, and the equivalent plastic strain ε = 0. For this time, Equation (8) can be simplified as:

$$\frac{\sigma}{KA} - 1 = C \ln \dot{\varepsilon}^* \tag{9}$$

According to the above formula, the C values of the different strain rates at the same temperature can be obtained, as shown in **Table 2**:

Table 2: Average value of C at fixed temperature

Temperature/°C	850	900	950
Average value of C	0.10058	0.1061	0.1027

According to the average value of C at different temperatures, the strain-rate sensitivity coefficient C = 0.1031 was determined.

3.1.3 Determination of temperature-softening index m and temperature-sensitivity coefficient D

When A, B, n and C are determined, Equation (1) can be transformed into:

$$1 - \frac{\sigma}{(A + B\varepsilon^n)(1 + C \ln \dot{\varepsilon}^*)} = DT^{*m} \tag{10}$$

The logarithm of Equation (10) is obtained:

$$\ln\left[1 - \frac{\sigma}{(A + B\varepsilon^n)(1 + C \ln \dot{\varepsilon}^*)}\right] = m \ln T^* + \ln D \tag{11}$$

Table 3: Average values of m and ln$D$ at fixed strain rates

strain rate s^{-1}	0.01	0.1	1	10
m	0.8544	0.71022	1.17447	1.0455
ln D	0.18307	0.12431	0.35321	0.30139

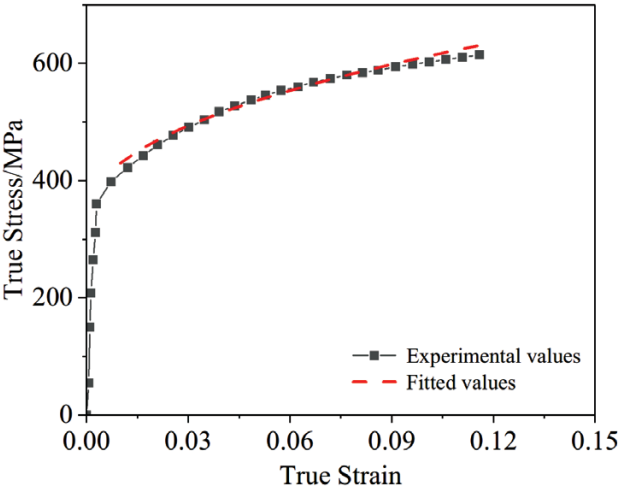

Figure 6: Comparison of experimental values and fitted values of true stress vs. true strain of materials at room temperature

According to the average value of m at different strain rates, the temperature-softening index m = 0.946 was determined. ln D = 0.24, D = 1.271.

The hot-deformation flow-stress model of 22MnB5 high-strength steel is obtained:

$$\sigma = (365+914.15\varepsilon^{0.55})\times[1+0.1031\ln(100\dot{\varepsilon})]\times \times\left(1-1.271\frac{T-25^{0.946}}{1445}\right) \quad (12)$$

3.1.4 Verification of Johnson-Cook constitutive equation

Figure 7 shows the comparison between the flow stress predicted by the Johnson-Cook constitutive model and the experimental data at different strain rates and different temperatures. It can be seen that the predicted value of the constitutive equation is in good agreement with the experimental value, which provides reliable material data for a subsequent finite-element simulation.

It can be seen from **Figure 7d** that the experimental value and the predicted value are basically distributed near the same straight line, indicating that the stress value predicted by the constitutive equation at different temperatures and different strain rates is basically consistent with the experimental value. In order to further verify the accuracy of the constitutive equation, the correlation coefficient R is introduced. The equation is:

$$R=\frac{\sum_{i=1}^{N}(\sigma_{Ei}-\overline{\sigma}_{E})(\sigma_{Pi}-\overline{\sigma}_{P})}{\sqrt{(\sigma_{Ei}-\overline{\sigma}_{E})^{2}(\sigma_{Pi}-\overline{\sigma}_{P})^{2}}} \quad (13)$$

where σ_{Ei} and $\overline{\sigma}_{E}$ denotes the average of the test value and the test value, respectively, in MPa, σ_{Pi} and $\overline{\sigma}_{P}$ denotes the mean value of predicted value and predicted value respectively, in MPa, and N represents the total number of data points.

The greater the R value, the better the fitting. The calculated R^2 = 0.985 shows that the Johnson-Cook constitutive model of 22MnB5 has high accuracy and can provide accurate data support for the numerical simulation.

3.2 Calculation and establishment of 22MnB5 hot-processing map

The material processing map is constructed based on the thermal deformation model. From the analysis of the

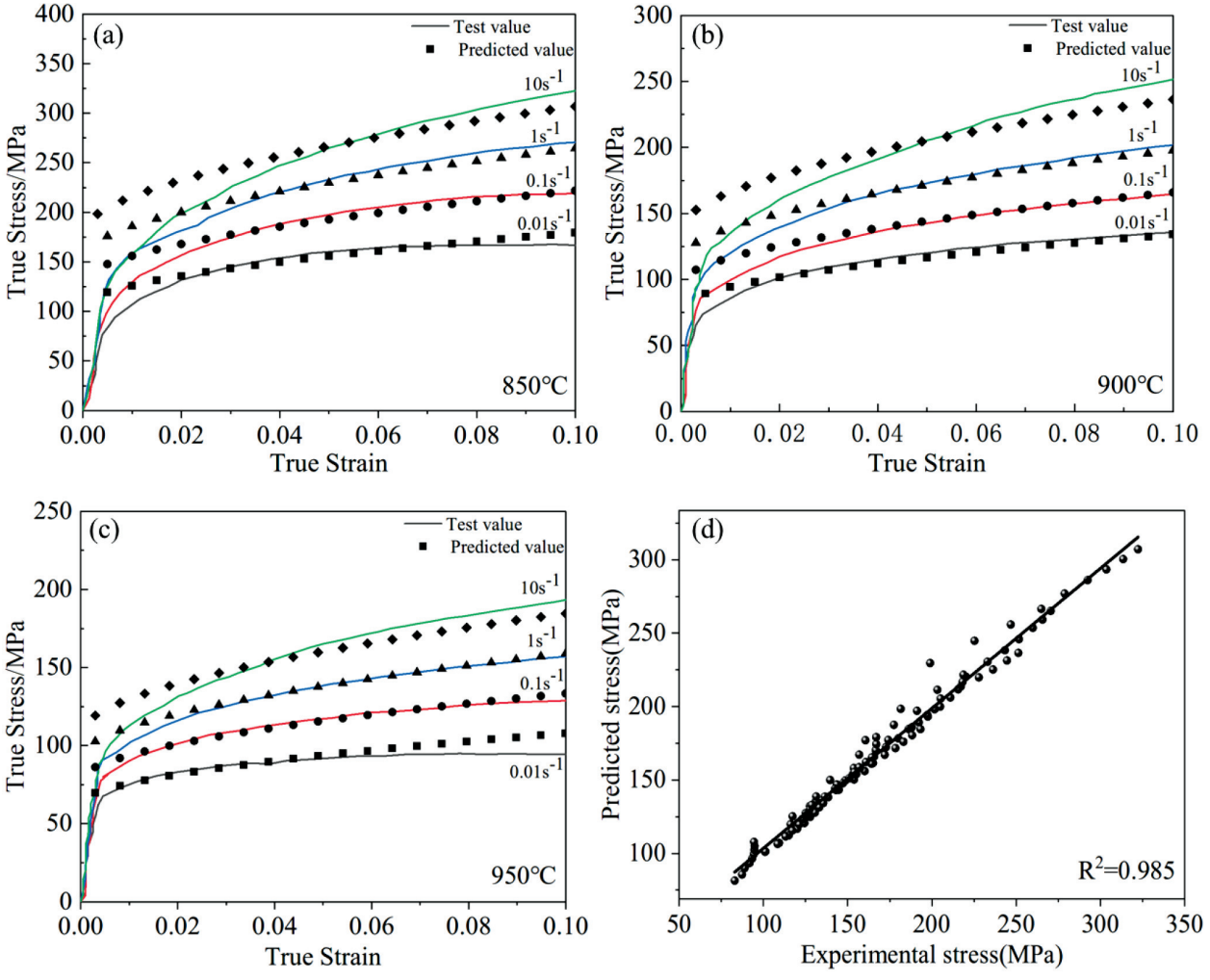

Figure 7: Comparison between predicted and experimental values for the flow stress of 22MnB5

composition diagram, the hot processing diagram is superimposed by the energy dissipation power diagram and the rheological instability diagram.[13,14] On the one hand, the hot-processing map can reflect the energy dissipation of the thermal deformation; on the other hand, it can indicate the 'stable zone' and 'unstable zone' of material processing.[15,16] This has a similar purpose to the establishment of the constitutive relation model of materials, both of which serve the thermal processing of materials. Through the hot-processing map, the processing performance of the material can be mastered, the microstructure can be controlled, and the defects can be avoided. It is of great significance for the optimization of the hot-processing process and the control of the microstructure of the material.[17,18]

The principle of the thermal processing map is that the total energy P obtained in the unit volume of the material during the processing process is composed of the energy G lost through plastic deformation and the energy J consumed by the evolution of the organization. G and J are called dissipation and dissipation, respectively. Its expression is as follows:

$$P = \sigma\dot{\varepsilon} = G + J = \int_0^{\dot{\varepsilon}} \sigma \mathrm{d}\dot{\varepsilon} + \int_0^{\dot{\varepsilon}} \dot{\varepsilon} \mathrm{d}\sigma \tag{14}$$

3.2.1 Strain-rate sensitivity exponent m

According to the stress and strain data, the logarithm of the stress and strain rate is selected when the strain is 0.04, 0.08, 0.12, 0.16, and the curves under different deformation temperature and deformation conditions are obtained, as shown in **Figure 8**.

The relationship between strain rate and stress is fitted by cubic polynomial, and its expression is:

$$\ln\sigma = a + b\ln\dot{\varepsilon} + c(\ln\dot{\varepsilon})^2 + d(\ln\dot{\varepsilon})^3 \tag{15}$$

where, a, b, c and d are the material correlation coefficients.

The strain rate sensitivity coefficient (m) is:

$$m = \frac{\partial \ln\sigma}{\partial \ln\dot{\varepsilon}} = b + 2c\ln\dot{\varepsilon} + 3d(\ln\dot{\varepsilon})^2 \tag{16}$$

The m-value response under different deformation conditions is shown in **Figure 9**.

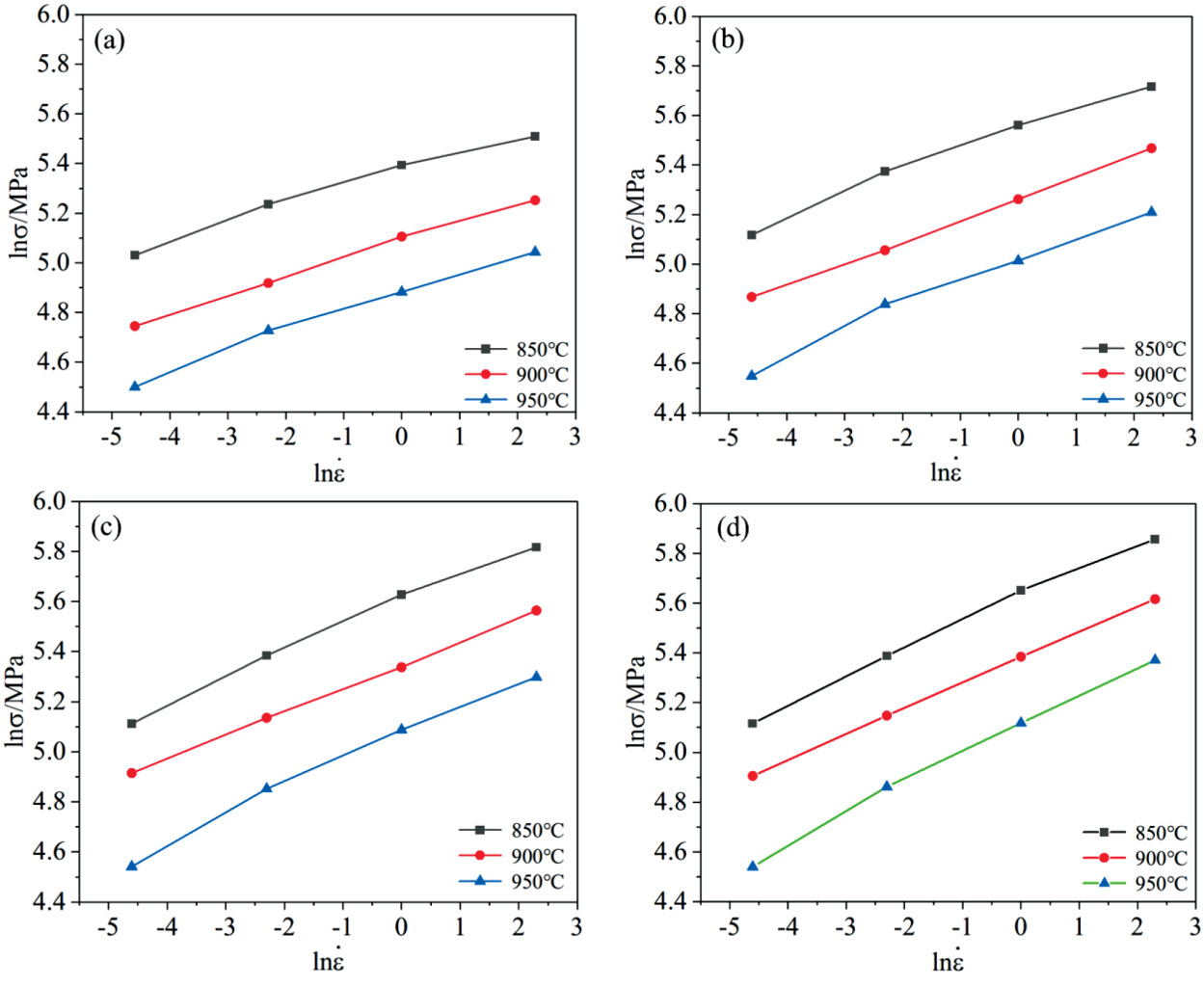

Figure 8: Relationship of hot-tensile deformation of 22MnB5 boron steel: a) 0.04, b) 0.08, c) 0.12, d) 0.16

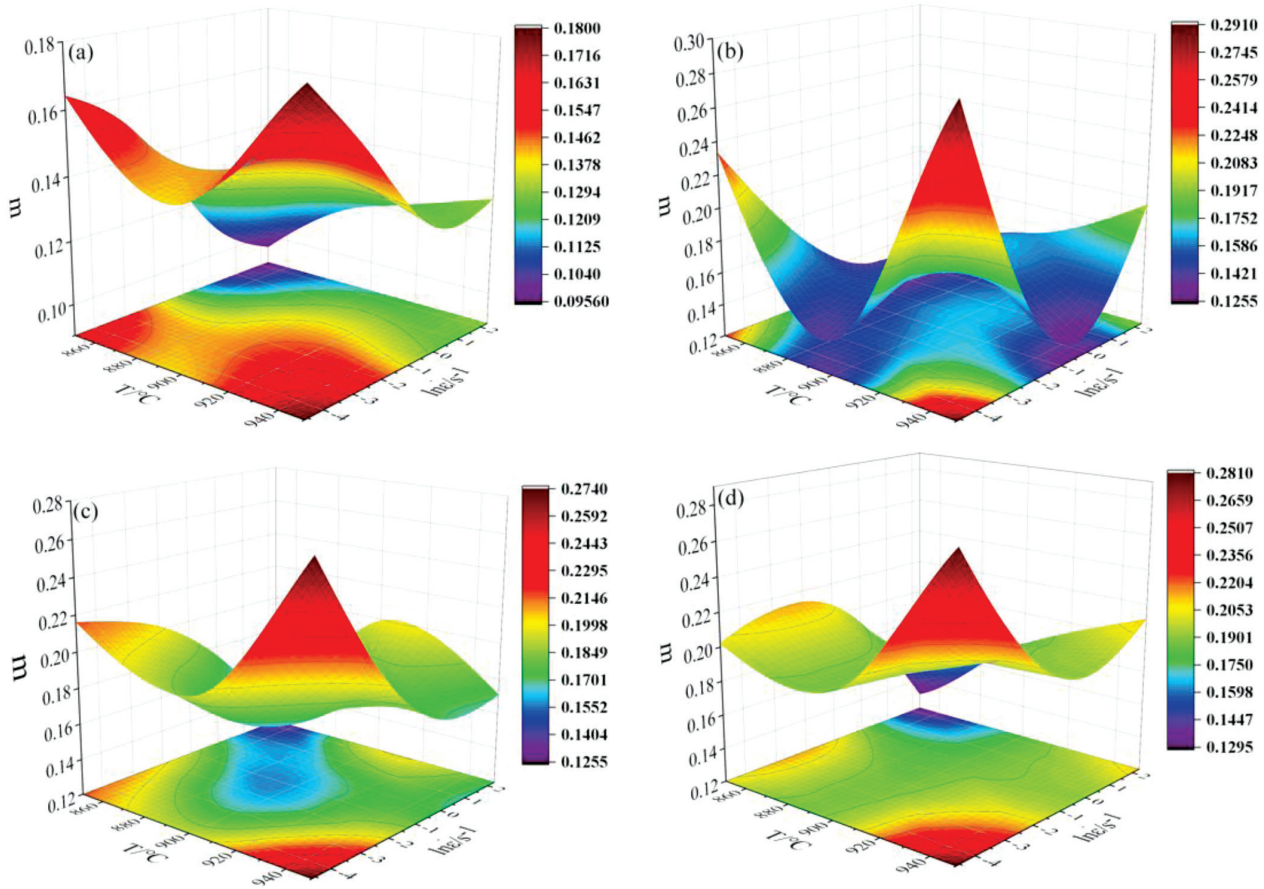

Figure 9: Response of m value to different deformation conditions under different strains: a) 0.04, b) 0.08, c) 0.12, d) 0.16

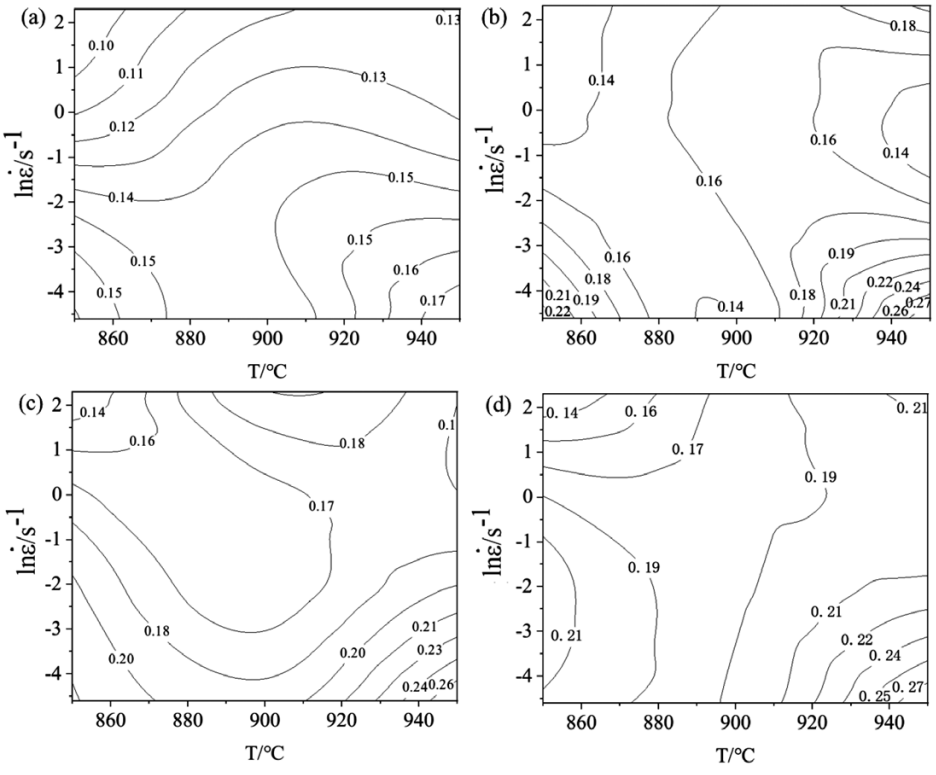

Figure 10: Power-dissipation diagram of 22MnB5 at different strains: a) 0.04, b) 0.08, c) 0.12, d) 0.16

It can be seen from the figure that the m value changes greatly under different deformation conditions, which indicates that the deformation mechanism inside the material is more complicated. There are many factors that affect the m value, such as surface slip, deformation twinning, etc. Therefore, the value of *m* cannot be used to judge the instability, and it is necessary to combine the power dissipation diagram and the instability diagram for further judgment.

3.2.2 Power-loss coefficient η

Figure 10 shows the change in the power-loss diagram with strain rate and deformation temperature, which plays an important role in guiding the selection of the optimal processing parameters in hot processing. According to the experimental data, the power-dissipation diagrams of 22MnB5 under different deformation degrees were established. The line in the figure is the equivalent curve, which represents the value of the power-loss coefficient η. Usually, the higher the η is, the easier the metal material processing deformation is.

It can be seen from **Figure 10** that when the strain is 0.04, most of the values are at a low level, less than 0.2. The results show that the value from low to high corresponds to the dynamic recrystallization process and the dynamic recovery process, respectively. With the increase of strain, the value gradually increases and the high value area gradually moves from the left side of the power-dissipation diagram to the right side, indicating that the increase of the temperature is beneficial to the processing of materials. With the increase of temperature, the dynamic recrystallization inside the material is more likely to occur, so the material at this time is more suitable for processing.

3.2.3 Instable judgement ζ(ε̇)

The instability criterion is expressed by parameter $\zeta(\dot{\varepsilon})$, which changes with the change of temperature and strain rate. When it is negative, it shows that the region belongs to the instability region, and the plastic instability of the processed material will occur in this region, indicating that this region is not suitable as a processing region. The expression of the instability criterion commonly used at present is:

$$\zeta(\dot{\varepsilon}) = \frac{\partial \ln\left(\frac{m}{m+1}\right)}{\partial \ln \dot{\varepsilon}} + m = \frac{2c + 6d(\ln \dot{\varepsilon})}{m(m+1)\ln 10} + m \qquad (17)$$

where $\zeta(\dot{\varepsilon})$ is the dimensionless instability parameter, $\dot{\varepsilon}$ is the strain rate, m is the strain-rate-sensitivity coefficient.

Figure 11 is the instability diagram of 22MnB5 under different strain conditions. The area where the contour value is less than 0 is the instability zone. When the strain is 0.04, the low-temperature (850 °C to 880 °C) and high-strain-rate (1 s^{-1} to 10 s^{-1}) region belongs to the instability region. When the strain is 0.08, the instability zone is concentrated in the region of T = 850 °C to 856 °C, 935 °C to 950 °C, $\dot{\varepsilon}$ = 0.01 s^{-1} to 1 s^{-1}; when the strain is 0.12 and 0.16, the instability zone is mainly con-

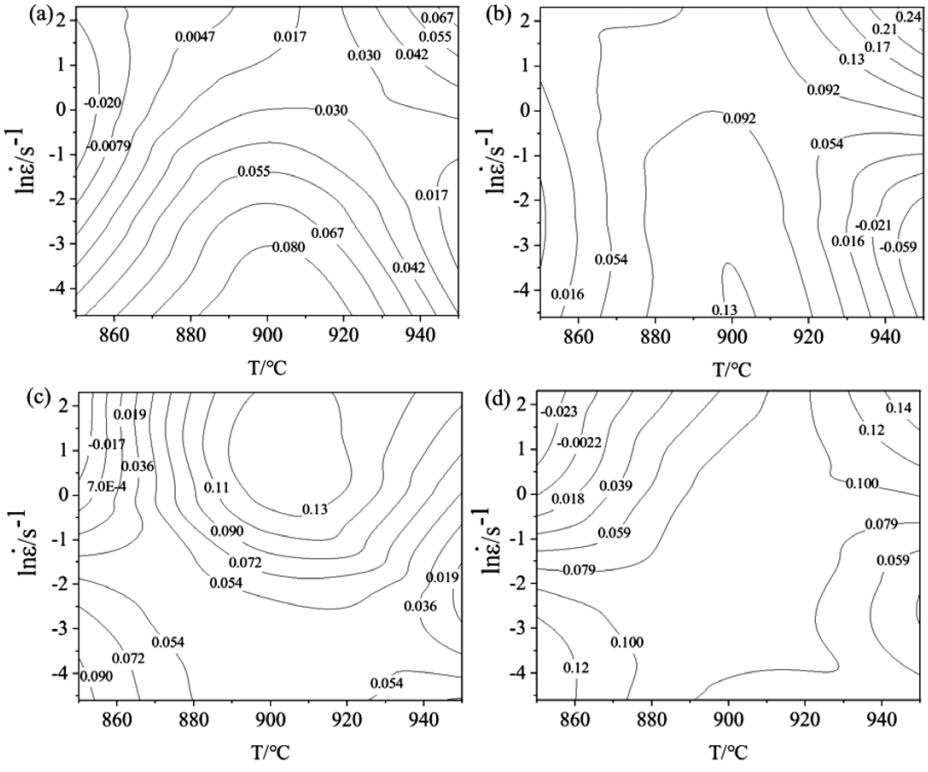

Figure 11: Instability diagram of 22MnB5 at different strains: a) 0.04, b) 0.08, c) 0.12, d) 0.16

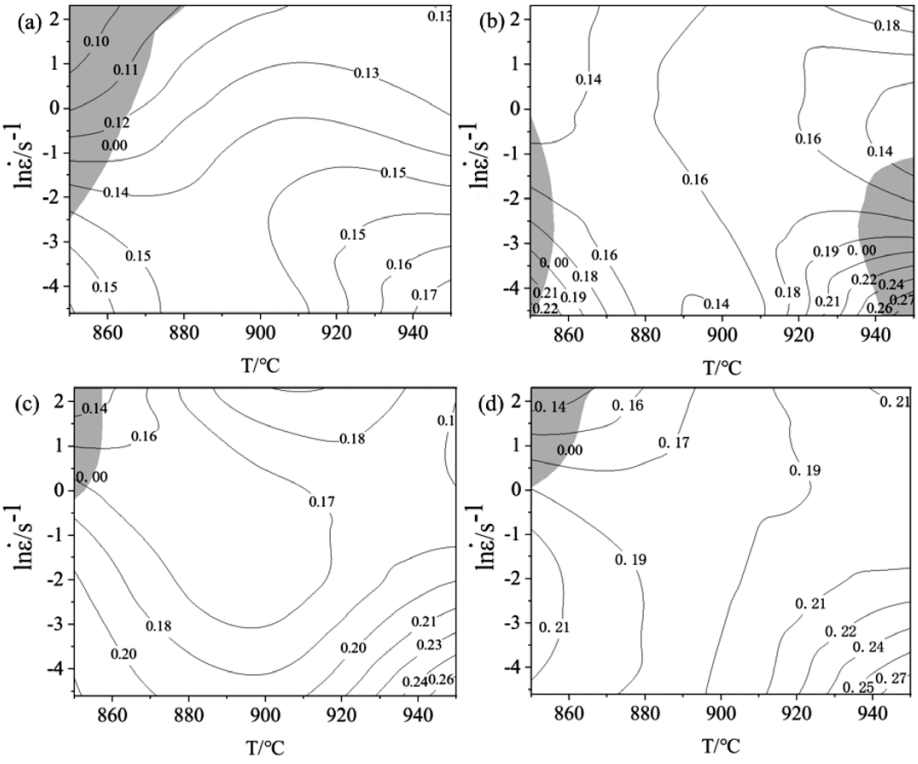

Figure 12: Hot-processing maps of 22MnB5 at different strains: a) 0.04, b) 0.08, c) 0.12, d) 0.16

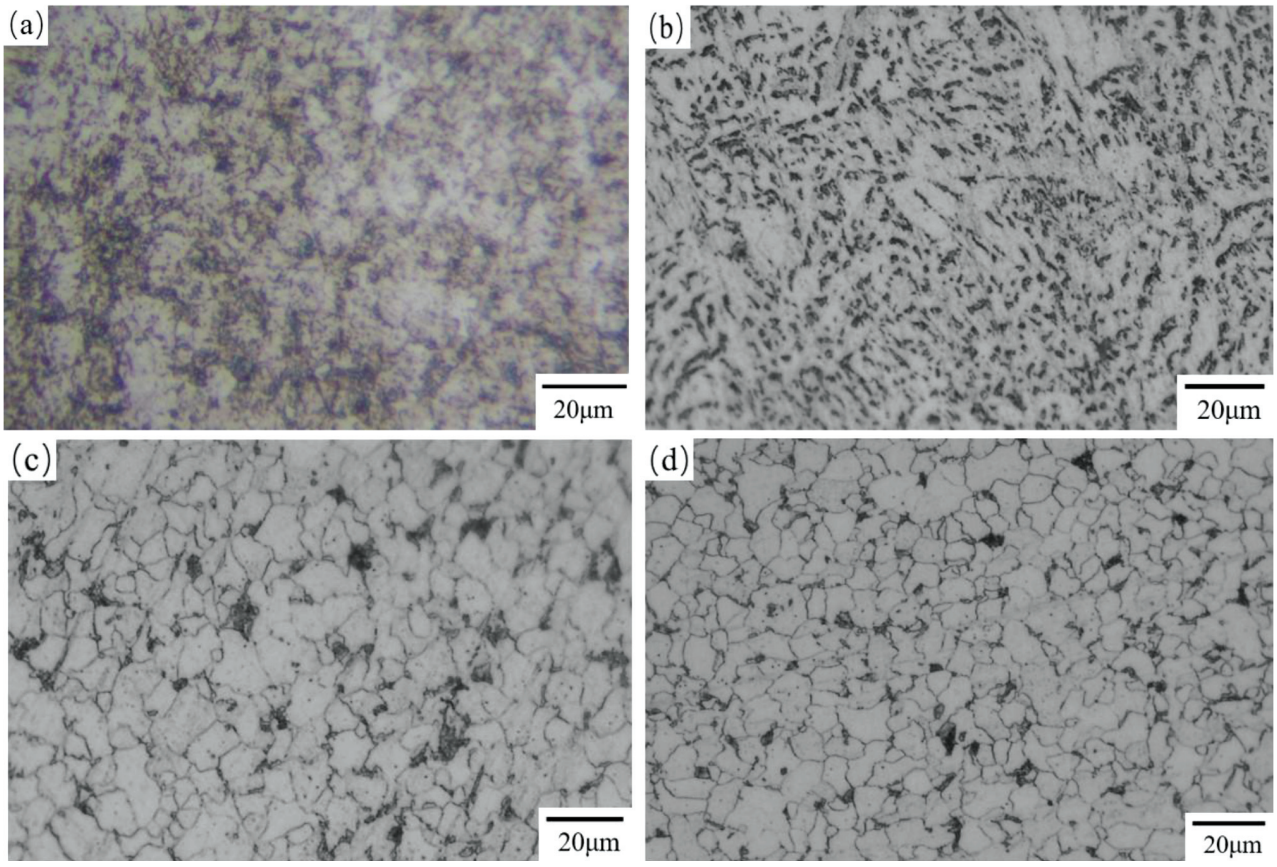

Figure 13: Microstructure of 22MnB5 after tensile fracture at different temperatures and strain rates: a) original structure, b) 950 °C, 0.1 s^{-1}, c) 850 °C, 10 s^{-1}, d) 900 °C, 1 s^{-1}

centrated in the T = 850 °C to 856 °C, $\dot{\varepsilon}$ = 1 s^{-1} to 10 s^{-1} region, and the area gradually increases. If the material is deformed in the unstable region, it might lead to flow instability, wedge cracking and adiabatic shear. Therefore, the instability region should be avoided during processing and it is necessary to combine the thermal processing map for analysis.

3.2.4 Establishment of hot-processing map

Consistent with the establishment of the power-dissipation diagram and the instability diagram, thermal processing maps with strains of 0.04, 0.08, 0.12 and 0.16 were established. **Figure 12** is a thermal processing map superimposed by power-loss diagram and an instability diagram. The gray area is the instability area, and the white area is the safety area. When the strain is 0.04, the instability region is mainly concentrated in the region of 850 °C to 875 °C and 0.1 s^{-1} to 10 s^{-1}.When the strain increases from 0.04 to 0.08, the instability region increases, mainly concentrated in the region of 850 °C to 855 °C, 0.01 s^{-1} to 1 s^{-1} and 935 °C to 950 °C, 0.01 s^{-1} to 0.34 s^{-1}.When the strain is 0.12 and 0.16, the area of the instability region decreases and is mainly concentrated in the region of low temperature and high strain rate. The power-loss coefficient decreases with the increase of strain rate, and the higher power-loss coefficient can improve the hot-deformation performance of the 22MnB5 high-strength steel. Therefore, the better process interval is 880 °C to 930 °C and the strain rate is 0.01 s^{-1} to 1 s^{-1}.

In order to verify the rationality of the thermal processing map, a cross-section of the original gauge area near the fracture of the high-temperature tensile specimen was cut, polished, and chemically etched. The etching agent was 4 % nitric acid alcohol solution, and the microstructure was observed by metallographic microscope after etching.

Figure 13 shows the microstructure of 22MnB5 steel under different deformation conditions. The recrystallization behavior of metallic materials is one of the main changes in the microstructure during hot deformation. The degree of dynamic recrystallization depends on strain, temperature and strain rate. **Figure 13a** shows the original microstructure of 22MnB5 sheet without heat treatment. It can be seen that the original microstructure of the sheet is ferrite (F) and pearlite (P). The cooling rate (20 °C/s) used in the hot tensile test is small, and the microstructure after cooling is ferrite, pearlite and a small amount of bainite. **Figures 13b**, **13c** and **13d** are the microstructure photographs at 950 °C, 0.1 s^{-1}, 850 °C, 10 s^{-1}, 900 °C , 1 s^{-1}, respectively, and **Figures 13b** and **13c** are in the instability zone of the hot-processing map. It can be seen that the structure of **Figure 13b** is ferrite and cementite distributed on the ferrite matrix. Cementite can improve the brittleness of steel, so it is not conducive to processing and forming. The microstructure of **Figure 13c** and **13d** is white ferrite and black pearlite. The dynamic recrystallization in **Figure 13c** is not enough, and some of the microstructure grows continuously at higher deformation temperatures, and finally becomes a coarse microstructure. Therefore, the figure is a mixed state of large grains and small grains. **Figure 13d** is in the non-instability region and the power-dissipation factor is high. The obtained grains are fine and the distribution is relatively uniform, which indicates that the metallographic structure diagram verifies the application rationality of the thermal processing map.

3.2.5 Fracture-morphology analysis of tensile specimen

According to the temperature and strain-rate range corresponding to the non-instability zone obtained from the hot-processing map, the tensile samples in the non-instability zone were selected, i.e., the samples with the deformation temperature of 900 °C and the strain rate of 1 s^{-1} were observed and analysed. It can be seen from the electron microscope image that the hot-tensile fracture is ductile fracture, and the fracture can be divided into fiber area and shear lip. The middle part of **Figure 14** is the fiber area, with round or oval dimples, and shear lips on both sides. Because the specimen is relatively thin, the fracture mode is a shear ductile fracture.

Figure 15 is the electron microscope picture of the fracture fiber area at different magnifications. It can be seen from the figure that the hot-stamping sample has obvious necking during stretching, and there are obvious delamination lines on both sides of the tensile fracture. There are a large number of dimples of different sizes in the fracture area, and there are inclusions in some dimples. During the tensile test, with the increase of stress, the sample first undergoes plastic deformation to produce necking. As the austenite grain boundary is destroyed, micro-cracks are generated in the necking area. Under the combined action of the increase in the number of micro-cracks and the hole-shaped cracks, when the stress increases to the critical value of fracture, the sample breaks.

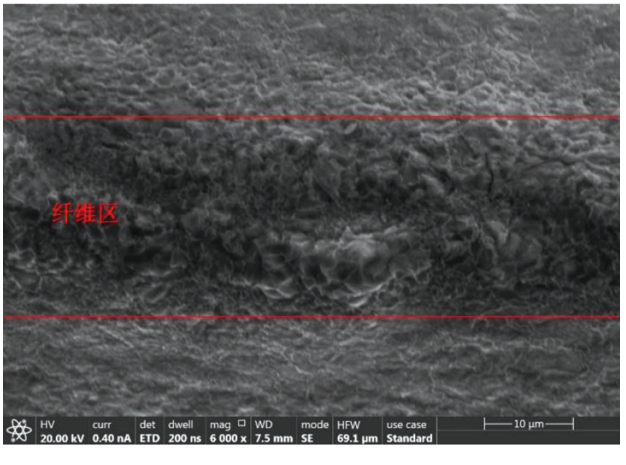

Figure 14: Fracture of high temperature tensile specimen

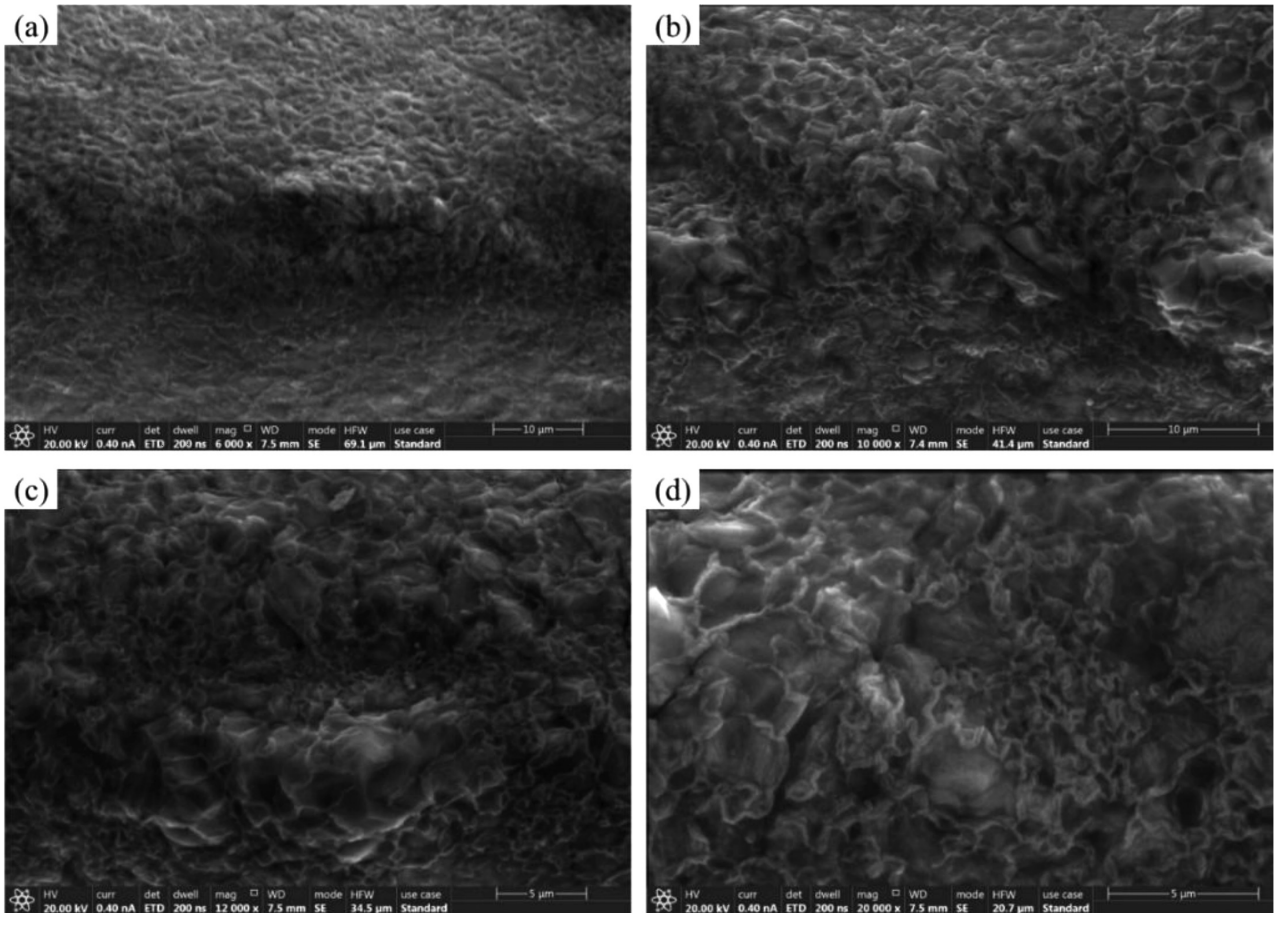

Figure 15: Microstructure of the fracture fiber zone at different magnifications: a) 6000×, b) 10,000×, c) 12,000×, d) 20,000×

4 CONCLUSIONS

1) Based on the high-temperature tensile test, the stress-strain curves of 22MnB5 at different temperatures and different strain rates were established. At the beginning of the deformation, the flow stress increased rapidly with the increase of strain. At this time, the deformation was dominated by work hardening. With the further increase of deformation, the flow stress tended to be stable after the work hardening and dynamic softening reached equilibrium.

2) An improved Johnson-Cook constitutive model of 22MnB5 high-strength steel was established based on the data obtained from high-temperature tensile test. The comparison between the constitutive model and the experimental data proves that the fitting effect is better. It shows that the established Johnson-Cook constitutive model has high accuracy and provides data support for a subsequent finite-element simulation.

3) Based on the dynamic material theory model (DMM), the power-dissipation diagram, instability diagram and thermal processing diagrams of 22MnB5 high-strength steel at different temperatures and strain rates were constructed. The instability zone is mainly concentrated at high strain rates at low temperatures and low strain rates at high temperatures, and the power dissipation coefficient decreases with increasing strain rate and increases with increasing temperature. Through analysis, the better process interval is 880 °C to 930 °C and the strain rate is $0.01s^{-1}$ to $1s^{-1}$.

Acknowledgment

This work is supported by the National Natural Science Foundation of China (51905501), this work is also supported by the Tangshan talent foundation innovation team (20130204D), Science and Technology Project of Hebei Education Department (QN2021117) funded by S&P Program of Hebei (Grant No.22281802Z).

5 REFERENCES

[1] X. F. Liu, Z. H. Jia, Q. Zhang, et al. Analysis on influencing factors of phase transformation inhomogeneity of synchronous quenching in hot stamping for ultra-high-strength steel plates [J]. Journal of Plasticity Engineering, 2019, doi:10.3969/j.issn.1007-2012.2019.02.033.

[2] M. Tomoyoshi, et al. Corner Strengthening by Local Thickening and Ausforming Using Planar Compression in Hot Stamping of Ultra-High Strength Steel Parts. Metals, 11.12(2021), doi:10.3390/MET11121977

[3] Z. Shao, N. Li, J. Lin, T. A. Dean, Strain measurement and error analysis in thermo-mechanical tensile tests of sheet metals for hot stamping applications. Proceedings of the Institution of Mechanical

Engineers, Part C: Journal of Mechanical Engineering Science, 2018, 232 (11), doi:10.1177/0954406217714011

[4] M. Maider, A. Garikoitz, G. Anton, et al. Effect of the Martensitic Transformation on the Stamping Force and Cycle Time of Hot Stamping Parts[J]. Metals – Open Access Metallurgy Journal, 2018, 8(6):385–398, doi:10.3390/met8060385

[5] T. Senuma, Y. Takemoto, T. Hojo, Control of Heterogeneous Microstructure for Improving Delayed Fracture Resistance of Ultrahigh Strength Hot Stamping Steel Sheets[J], Tetsu-to-Hagane, 2019, 105(2):173–181, doi:10.2355/tetsutohagane.TETSU-2018-079

[6] D. He, X.-T. Yan, Y. C. Lin, S. Zhang, Z.-J. Chen, Microstructure evolution and constitutive model for a Ni-Mo-Cr base alloy in double-stages hot compression with step-strain rates. Materials Characterization, 2022, 194, doi:10.1016/J.MATCHAR.2022.112385

[7] Y. C. Lin, D. X. Wen, J. Deng, G. Liu, J. Chen, Constitutive models for high-temperature flow behaviors of a Ni-based superalloy, Materials and Design, 2014, 59(9):115-123, doi:10.1016/j.matdes.2014.02.041

[8] Z. Jing, Z. Song, L. I. Binxun, Modified J-C constitutive model of H13 steel based on reverse fitting algorithm [J], Journal of Central South University (Science and Technology), 2019, doi:10.11817/j.issn.1672-7207.2019.08.007

[9] Y. C. Lin, J. Deng, Y.-Q. Jiang, D.-X. Wen, G. Liu, Effects of initial δ phase on hot tensile deformation behaviors and fracture characteristics of a typical Ni-based superalloy, Materials Science & Engineering A, 2014, 598, doi:10.1016/j.msea.2014.01.029

[10] Y. C. Lin, S. C. Luo, X. Y. Jiang, et al., Hot deformation behavior of a Sr-modified Al-Si-Mg alloy: Constitutive model and processing maps, Transactions of Nonferrous Metals Society of China, 2018, 28(4):592–603, doi:10.1016/S1003-6326(18)64692-8

[11] A. Turetta, S. Bruschi, A. Ghiotti. Investigation of 22MnB5 formability in hot stamping operations. Journal of Materials Processing Technology, 2006, 177(1–3):396-400, doi:10.1016/j.jmatprotec.2006.04.041

[12] Z. Jing, B. Wang, M. Huang, Two constitutive descriptions of boron steel 22MnB5 at high temperature. Materials & Design, 2014, 63(nov.):738-748. doi:10.1016/j.matdes.2014.07.008

[13] O. B. Bembalge, S. K. Panigrahi, Hot deformation behavior and processing map development of cryorolled AA6063 alloy under compression and tension. International Journal of Mechanical Sciences, 2021, 191:106100, doi:10.1016/j.ijmecsci.2020.106100

[14] He, Dao-Guang, Lin, et al., Effect of pre-treatment on hot deformation behavior and processing map of an aged nickel-based superalloy. Journal of Alloys & Compounds, 2015, doi:10.1016/j.jallcom.2015.07.213

[15] J. Yu, Z. Li, C. Qian, S. Huang, H. Xiao, Investigation of deformation behavior, microstructure evolution, and hot processing map of a new near-α Ti alloy, Journal of Materials Research and Technology, 2023, 23, doi:10.1016/J.JMRT.2023.01.177

[16] C. Liu, S. Barella, Y. Peng, S. Guo, S. Liang, J. Sun, A. Gruttadauria, M. Belfi, C. Mapelli, Modeling and characterization of dynamic recrystallization under variable deformation states, International Journal of Mechanical Sciences, 2023, 238, doi:10.1016/J.IJMECSCI.2022.107838

[17] D. Mirahmadi, K. Dehghani, A. Shamsipur, A. Kalaki, Hot deformation behavior, microstructure evolution and processing map of Cu–2Be alloy. Journal of Materials Research and Technology, 2023, 24, doi:10.1016/J.JMRT.2023.02.215

[18] S. Q. Wang, X. Zhao, X. W. Ren, Z. M. Zhang, X. D. Tian, Y. Y. He, Hot Deformation Behavior and Processing Map Considering Strengthening Effect for Al–10.0Zn–3.0Mg–2.8Cu Alloy[J], Materials, 2023, 16(5), doi:10.3390/MA16051880